Inorganic Chemistry

Article

pubs.acs.org/IC

Cu_3I_7 Trimer and Cu_4I_8 Tetramer Based Cuprous Iodide Polymorphs for Efficient Photocatalysis and Luminescent Sensing: Unveiling Possible Hierarchical Assembly Mechanism

Shi-Li Li and Xian-Ming Zhang*

School of Chemistry & Material Science, Shanxi Normal University, Linfen, Shanxi 041004 China

Supporting Information

ABSTRACT: Solvothermal reactions of CuI, 1,4-diazabicyclo[2.2.2]octane (DABCO), and HI in an ethanol solution at 140 °C/150 °C for 7 days resulted in two 24-membered-ring-based layered semiconducting iodocuprate open-network polymorphs formulated as $[deDABCO]_2[meDABCO]Cu_{11}I_{17}$ (deDABCO = *N*,*N*′-diethyl-1,4-diazabicyclo[2.2.2] octane and meDABCO = *N*-methyl-*N*′-ethyl-1,4-diazabicyclo[2.2.2]octane). The deDABCO and meDABCO templates were in situ generated via alkylation of DABCO during solvothermal reactions. The formation of layered $Cu_{11}I_{17}^{6-}$ polymorphs can be rationalized via analyses of hierarchical building units. There are four hierarchical building units in polymorphs, namely, primary CuI_3 triangle and CuI_4 tetrahedron, secondary Cu_3I_7 trimer and Cu_4I_8 tetramer, tertiary Cu_6I_{12} hexamer, and quaternary $Cu_{12}I_{22}$ dodecamer. The trimeric Cu_3I_7 secondary building unit (SBU) is constructed by three edge-shared CuI_4 tetrahedra, while the tetrameric Cu_4I_8 SBU with an inversion center is formed by edge-shared two CuI_3 triangles and two CuI_4 tetrahedra. Two Cu_3I_7 SBUs are fused together via the sharing of two iodine atoms to form a Cu_6I_{12} tertiary building unit (TBU), and two TBUs are further fused via the sharing of two iodine atoms into a $Cu_{12}I_{22}$ quaternary building unit (QBU). In colorless polymorph **1**, each Cu_3I_7 SBU is connected to three neighbors via one Cu_4I_8 and two Cu_6I_{12} linkers to form a 6,3-connected layer with 24-membered ring window. Different from **1**, each Cu_6I_{12} TBU in yellowish polymorph **2** is connected to four neighbors via two Cu_4I_8 and two $Cu_{12}I_{22}$ linkers to form a (4,4) topological layer also with 24-membered-ring window. These two compounds are very rare examples of copper halide polymorphs that exhibit similar local coordination geometries of copper(I) but different layered open networks. Electrical conductivity, band structure calculation, and UV−vis diffuse-reflectance spectrometry indicate that **1** and **2** are potential semiconductor materials, and the performance on the photocatalytic degradation of organic pollutants upon UV-light irradiation reveals that both **1** and **2** are highly efficient photocatalysts. Two polymorphs exhibit very similar green photoluminescence at room temperature in the solid state, and the study of the luminescent response to solvent on two polymorphs exhibits highly sensitive sensing of nitro explosives via quenching.

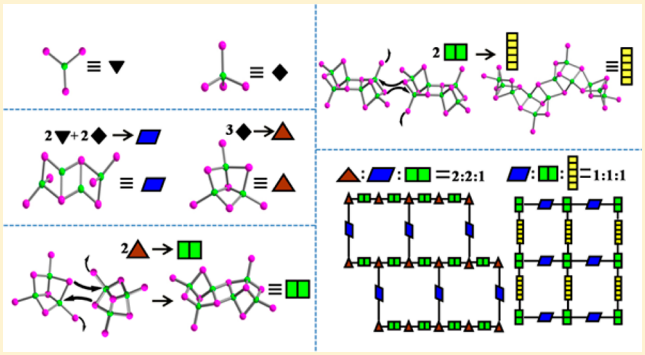

INTRODUCTION

Polymorphism, the same chemical composition existing in more than one crystalline structure, is of great importance in molecular crystals, coordination polymers, inorganic materials, and organic−inorganic hybrids.[1] Polymorphs often show remarkably different physical and chemical properties, giving unique insight on the structure−property relationship. For example, only a fraction of polymorphs are active pharmaceutical ingredients in drug products.[2] In inorganic materials, silicoaluminate polymorphs with the same chemical composition have different superstructures and applications ranging from catalysts to adsorbents.[3] In addition, well-known carbon materials including diamond, graphite, graphene, and carbon nanotube display very different applications such as extraordinary electrical, thermal, and physical properties.[4] Control over polymorphs lies at the very heart of the concept of crystal engineering. Polymorphs can provide useful information on the controlled growth of single crystals as well as on the structure−property relationship.[5] However, there is presently very little understanding concerning the existence and control over polymorphs.[6] Nevertheless, some knowledge concerning the mechanism of formation and the control of crystal growth has been cumulated in the field of inorganic materials.[7] For instance, microporous zeolites as petroleum cracking catalysts have been continuously explored, and the mechanism for their formation has been proposed. It is generally thought that TO_4 tetrahedra (T = Al, Si) are initial building units in silicoaluminate zeolites,[8] which can aggregate into ring-shaped tetramer T_4O_{12} and hexamer T_6O_{18}, etc., secondary building units (SBUs) that are further assembled into tertiary building units (TBUs). These hierarchical building units as nucleation

Received: April 15, 2014
Published: July 25, 2014

   dx.doi.org/10.1021/ic500822w | Inorg. Chem. 2014, 53, 8376−8383

agents in solution are organized in intricately oriented ways to form various silicoaluminate polymorphs with molecular-sieve properties.[9]

Mimicking of silicoaluminate zeolites and mineral materials by other inorganic materials is of intense current interest. Analogous to silicoaluminate zeolites, copper(I) halide aggregates represent a truly potential family in the construction of polymorphs because only a subtle difference in energy is found in the chemically equivalent aggregates of different geometries. In addition to pores, copper halides can contribute to the luminescence, ionic conductivity, and high reactivity in numerous organic and biochemical reactions.[10] It is well-known that the coordination modes of copper(I) and halide atoms are more flexible than those of T and O in silicoaluminates, resulting in much richer SBUs such as Cu_2X_2,[11] Cu_3X_3,[12] Cu_3X_7,[13] Cu_3X_8,[14] Cu_4X_4,[15] Cu_4X_{11},[16] Cu_4X_9,[17] Cu_6X_6,[18] and so on. Neutral copper(I) halide SBUs such as Cu_2X_2, Cu_4X_4, and Cu_6X_6 can be linked by organic ligands to form copper(I) halide coordination polymers, while anionic SBUs can assemble into organic-templated copper halide frameworks. Structurally, organic-templated copper halide frameworks are very closely similar to silicoaluminate zeolites. Thus, one may expect that copper halide SBUs in combination with TBUs and even QBUs can be fused via the sharing of halides to form copper halide frameworks similar to silicoaluminate zeolites. Unfortunately, the realization on SBUs, TBUs, and QBUs and their forming and assembling mechanism in copper halides are still ambiguous and have rarely been discussed ever before. Coordinative flexibility, high reactivity, and semiconducting behavior as well as distinguished luminescent properties encourage us to investigate cuprous halide polymorphs and the hierarchical assembly mechanism.[10e,20] Fortunately, two layered 24-membered-ring open-network polymorphs $(deDABCO)_2(meDABCO)Cu_{11}I_{17}$, **1** and **2**, have been prepared, in both of which Cu_3I_7 trimer and Cu_4I_8 tetramer function as SBUs that are further fused into hexameric Cu_6I_{12} TBUs. In yellowish polymorph **2**, Cu_6I_{12} TBUs are even aggregated into dodecameric $Cu_{12}I_{22}$ QBUs. On the basis of these observations, a hierarchical model for forming and assembling copper halide frameworks has been proposed. The electrical resistivity and UV−vis diffuse-reflectance measurements as well as band structure calculations reveal that **1** and **2** possess semiconductor behavior, and both polymorphs are highly efficient heterogeneous photocatalysts under UV light. Interestingly, both polymorphs exhibit solvent-dependent photoluminescence and highly sensitive sensing of nitrobenzene (NB) explosives through a fluorescence quenching mechanism.

EXPERIMENTAL SECTION

Materials and Methods. The Fourier transform infrared (FT-IR) spectra were recorded from KBr pellets in the range 400−4000 cm^{-1} on a PerkinElmer Spectrum BX FT-IR spectrometer. Elemental analysis was performed on a Vario EL-II elemental analyzer. Powder X-ray diffraction (PXRD) data were recorded in a Bruker D8 ADVANCE powder X-ray diffractometer (Cu Kα, λ = 1.5418 Å). Photoluminescence analysis was performed on an Edinburgh FLS920 luminescence spectrometer. UV−vis absorption was monitored with a U-3310 spectrophotometer. Electrical resistivity measurements were performed on rectangular-shaped pressed pellets (two probes) using a ZLS-LCR conductometer.

Syntheses. A mixture of copper iodide (CuI), 1,4-diazabicyclo[2.2.2]octane (DABCO), hydroiodic acid (HI), and ethanol (EtOH) in a molar ratio of 5:2:7:150 was sealed in a 15-mL Teflon-lined stainless container, which was heated to 140 °C for 7 days. With a cooling rate of 5 °C min^{-1} to room temperature, colorless crystals of **1** in 56% yield were recovered, while yellowish crystals of **2** in 39% yield were obtained by using a similar procedure at 150 °C. Anal. Calcd for **1** $C_{30}H_{50}Cu_{11}I_{17}N_6$: C, 10.74; H, 1.49; N, 2.51. Found: C, 10.86; H, 1.56; N, 2.36. IR (KBr, cm^{-1}): ν 3436(s), 2987(w), 1633(s), 1459(s), 1395(m), 1189(w), 1110(s), 1062(w), 967(w), 930(w), 847(s), 798(m), 612(w). Anal. Calcd for **2** ($C_{30}H_{50}Cu_{11}I_{17}N_6$): C, 10.74; H, 1.49; N, 2.51. Found: C, 10.91; H, 1.54; N, 2.31. IR (KBr, cm^{-1}): ν 3436(s), 2987(w), 2913(w), 1628(s), 1453(s), 1279(w), 1199(w), 1115(m), 1057(w), 972(w), 935(w), 845(m), 728(w), 612(w).

Photocatalytic Experiments. For photocatalytic activity measurement, 30 mg each of compounds **1** and **2** were added to 30 mL of a 1×10^{-5} mol L^{-1} solution of Methyl Orange (MO), Methylene Blue (MB), and Erioglaucine Disodium salt (ED), a 5×10^{-5} mol L^{-1} solution of Azure I (AI) and Eosin Y (EY), and a 1×10^{-4} mol L^{-1} solution of Neutral Red (NR) and Malachite Green (MG). The suspensions were magnetically stirred in the dark for 30 min to ensure adsorption equilibrium and uniform dispersity. The solution was then exposed to UV irradiation from a 125-W high-pressure mercury lamp, with the strongest emission at room temperature. After a given irradiation time, 5 mL of the mixture was withdrawn, and the catalysts were separated from the suspensions by centrifugation. The degradation process was monitored through a wavelength scan on a U-3310 spectrophotometer.

Calculation Details. The electronic band structures along with density of states (DOS) for **1** and **2** were calculated by density functional theory (DFT) using the crystallographic data with the CASTEP code, which uses a plane-wave basis set for the valence electrons and norm-conserving pseudopotential for the core electrons.[19] The number of plane waves included in the basis set was determined by a cutoff energy E_c of 351 eV. The parameters used in the calculations and convergence criteria were set by the default values of the CASTEP code, for example, an eigen-energy convergence tolerance of 1.0×10^{-5} eV.

Crystallographic Studies. Single-crystal X-ray diffraction data for **1** and **2** were collected on a Agilent Technologies Gemini EOS diffractometer at 298 K using Mo Kα radiation (λ = 0.71073 Å). The program *SAINT* was used for integration of diffraction profiles, and the program *SADABS* was used for absorption correction. The structures were solved with the *XS* structure solution program by direct methods and refined by a full-matrix least-squares technique using *Olex2*. All non-hydrogen atoms were refined with anisotropic thermal parameters. Hydrogen atoms of organic cations were generated theoretically onto the specific carbon atoms and refined isotropically with fixed thermal factors. The crystallographic data are listed in Table 1. Selected bond lengths and bond angles are given in Table S1 in the Supporting Information (SI).

RESULTS AND DISCUSSION

Description of Structures. Colorless polymorph **1** crystallizes in monoclinic space group $P2_1/n$, and the asymmetric unit consists of 11 crystallographically independent copper(I) ions, 17 iodides, and one *N*-methyl-*N*′-ethyl-1,4-diazabicyclo[2.2.2]octane (meDABCO) and two *N*,*N*′-diethyl-1,4-diazabicyclo[2.2.2]octane (deDABCO) groups. Both meDABCO and deDABCO groups came from in situ alkylation of DABCO. In the course of formation, the N-heterocyclic DABCO groups were in situ reacted with alcohols to form N-alkylated cations, which played a key role in the self-assembly reaction of anionic frameworks. The formation mechanism of in situ alkylation is suggested as follows: under high temperature and autogenous pressure, the nucleophilic substitution reaction of alcohols and aqueous HI can generate alkyl iodides, which attack the nitrogen atom of DABCO to form the quaternary ammonium ions. This kind of mechanism of the in situ alkylation reaction has also been discussed by our

dx.doi.org/10.1021/ic500822w | Inorg. Chem. 2014, 53, 8376−8383

Table 1. Crystallographic Data and Structure Refinement for 1 and 2

	1	2
formula	$C_{29}H_{63}Cu_{11}I_{17}N_6$	$C_{29}H_{63}Cu_{11}I_{17}N_6$
fw	3352.00	3352.00
cryst syst	monoclinic	triclinic
space group	$P2(1)/c$	$P\bar{1}$
a (Å)	11.3994(3)	11.3280(7)
b (Å)	22.7376(5)	15.3667(8)
c (Å)	26.6703(7)	19.9816(12)
α (deg)	90	78.509(5)
β (deg)	96.499(2)	85.582(5)
γ (deg)	90	84.045(4)
V (Å^3)	6868.4(3)	3384.5(3)
Z	4	2
ρ_{calcd}(g cm^{-3})	3.242	3.289
μ (mm^{-1})	11.000	11.162
F(000)	5996	2998
reflections	31912/13479	27580/13792
T_{max}/T_{min}	0.2892/0.1267	0.2853/0.1668
data/param	13479/7/578	13792/40/568
S	1.057	1.046
R1[a]	0.0397	0.0474
wR2[b]	0.0892	0.1011
$\Delta\rho_{max}/\Delta\rho_{min}$(e A^{-3})	1.527/−1.332	2.016/−2.219

[a] $R1 = \sum||F_o| - |F_c||/\sum|F_o|$. [b] $wR2 = [\sum[w(F_o^2 - F_c^2)^2]/\sum[w(F_o^2)^2]]^{1/2}$.

and other groups,[14,20] and the reason for the formation of different N-alkylated cations might be that the C−C bond of EtOH is broken in an alkylated reaction or there is a small amount of methanol in a commercially available EtOH solution. All of the copper(I) ions show tetrahedral coordination geometries except that Cu1 is in a slightly distorted triangular planar site (Figure 1a). Triangular-coordinated Cu1 is coordinated by two μ_3-iodine and one μ-iodine atoms with Cu−I distances of 2.5246(16)−2.6685(17) Å and I−Cu−I angles of 106.70(6)−126.25(7)°. The remaining copper(I) ions are coordinated by four iodine atoms with Cu−I distances of 2.487(7)−2.950(11) Å and I−Cu−I angles of 99.61(5)−138.7(7)°. The Cu···Cu distances are in the range of 2.50(2)−3.0574(17) Å, in which the remarkably short Cu···Cu distance of 2.50(2) Å is caused by disordered copper atoms, indicative of the presence of weak Cu···Cu interactions. The structure of **1** possesses an unprecedented anionic layered open framework constructed by the two basic building units Cu_3I_7 and Cu_4I_8 (Figure 2). The Cu_3I_7 trimer is constructed by three edge-shared CuI_4 tetrahedra. The Cu_4I_8 unit has an inversion center and is formed by edge-shared two CuI_3 triangles and two CuI_4 tetrahedra, in which a triangle is edge-shared with a triangle and a tetrahedron while a tetrahedron is only edge-shared with a triangle. The layer can be simply described as a (6,3) topological network, in which the nodes are Cu_3I_7 trimers (Figure 3a). There are two types of connectors: one is the Cu_4I_8 tetramer, and the other is the Cu_6I_{12} hexamer, which is constructed from two Cu_3I_7 trimers via the sharing of two iodides. Each Cu_3I_7 node is connected to three adjacent nodes via one Cu_4I_8 unit and two Cu_6I_{12} units. As a result, the $Cu_{11}I_{17}^{6-}$ layer creates a 24-membered-ring cavity sized at ca. 28.17 Å. The cavity and interlayer are occupied by alkylated meDABCO and deDABCO groups to compensate for charge (Figure S1 in the SI).

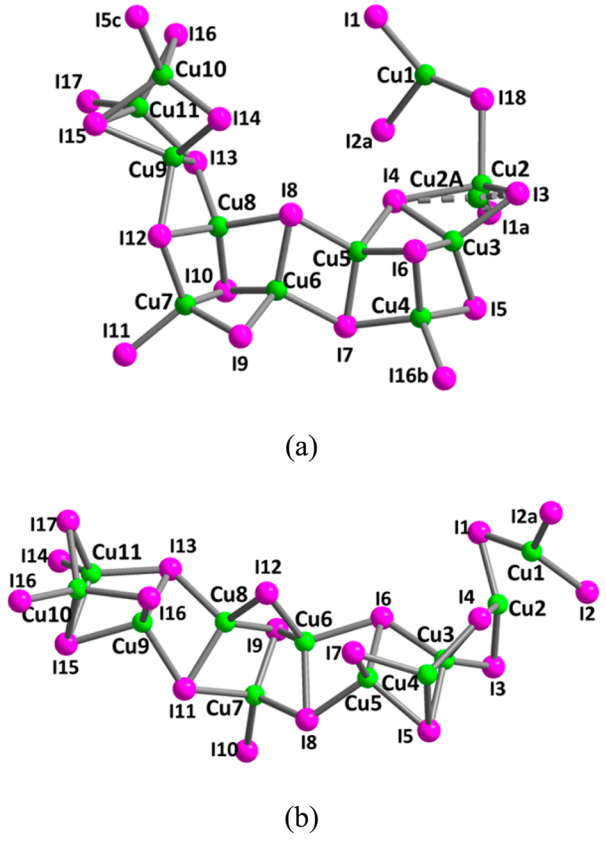

Figure 1. View of the coordination environments of copper(I) atoms in **1** (a) and **2** (b).

Yellowish polymorph **2** crystallizes in triclinic $P\bar{1}$, and the asymmetric unit also consists of 11 crystallographically independent copper(I) ions, 17 iodides, and one meDABCO and two deDABCO groups, as shown in Figure 1b. Cu1 is tricoordinated with Cu1−I distances in the range of 2.525(2)−2.662(2) Å and I−Cu1−I angles of 106.92(8)−127.10(8)°, similar to the Cu1 atom in polymorph **1**. The other 10 copper atoms are tetrahedrally coordinated, with Cu−I distances of 2.507(2)−3.057(3) Å and I−Cu−I angles of 97.05(8)−135.71(11)°. Compared with **1**, the Cu···Cu distances vary in a smaller range of 2.534(3)−2.957(3) Å (average 2.814 Å) due to the absence of a disordered copper atom. Similar to **1**, the SBUs also are Cu_3I_7 trimers and Cu_4I_8 tetramers. Quite differently, two hexameric Cu_6I_{12} TBUs are further aggregated into a docecameric $Cu_{12}I_{22}$ QBU. The overall layer is also formulated as $Cu_{11}I_{17}^{6-}$ with 24-membered-ring cavities. Distinguished from **1**, polymorph **2** shows a wavelike (4,4) layer constructed by Cu_6I_{12} nodes and Cu_4I_8 and $Cu_{12}I_{22}$ linkers.

Polymorphism, which can be considered a specific subset of supramolecular isomerism, is particularly rare for copper halides with inorganic frameworks.[21] In **1** and **2**, the local coordination spheres of copper(I) cations are the same, and the basic building blocks are similar. The significant difference originates from four kinds of aforementioned hierarchical building units including $Cu_{12}I_{22}$ QBU in **2** and Cu_3I_7 SBU, Cu_4I_8 SBU, and Cu_6I_{12} TBU in **1** and **2**. It should be pointed out that Cu_3I_7 SBU has been revealed in mixed-valent $[Cu^{II}_2Cu^{I}_7I_{14}]^{3-}$,[13,22] while Cu_4I_8 SBU, Cu_6I_{12} TBU, and $Cu_{12}I_{22}$ QBU have not been documented before the work. Because of different connecting modes of these hierarchical building units in two polymorphs, a

dx.doi.org/10.1021/ic500822w | Inorg. Chem. 2014, 53, 8376−8383

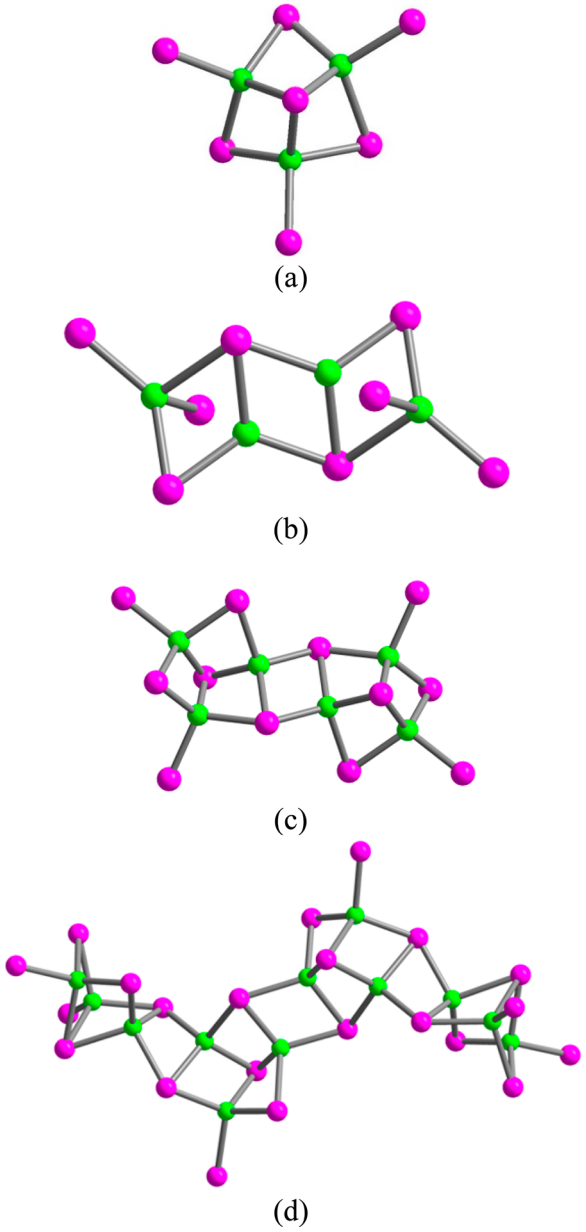

Figure 2. View of the Cu_3I_7 trimer (a), Cu_4I_8 tetramer (b), Cu_6I_{12} hexamer, (c) and $Cu_{12}I_{22}$ dodecamer building units.

herringbone-like network in **1** and bricklike networks in **2** are formed (Figures 3 and 4). It is obvious that, from a topological point of view, the herringbone-like and bricklike networks show significantly different arrangements of (6,3) and (4,4) layers, both of which consist of similar 24-membered rings and are stabilized by alkylated cations via C−H···I hydrogen bonds.[23] Polymorphs **1** and **2** were generated from the solvothermal reaction of CuI, DABCO, and HI in an EtOH solution at 140 and 150 °C for 7 days, respectively. With an increase in the synthesis temperature to 160 °C, no crystalline phases were generated under the same synthetic conditions. When the reaction temperature was decreased to 130 °C, two kinds of crystals with distinct differences in yield and morphology, a large amount of block crystals **1**, and a small amount of needlelike crystals $(DeDABCO)_2[Cu_4I_8]^{20c}$ were simultaneously formed by a one-pot solvothermal reaction. Thus, two

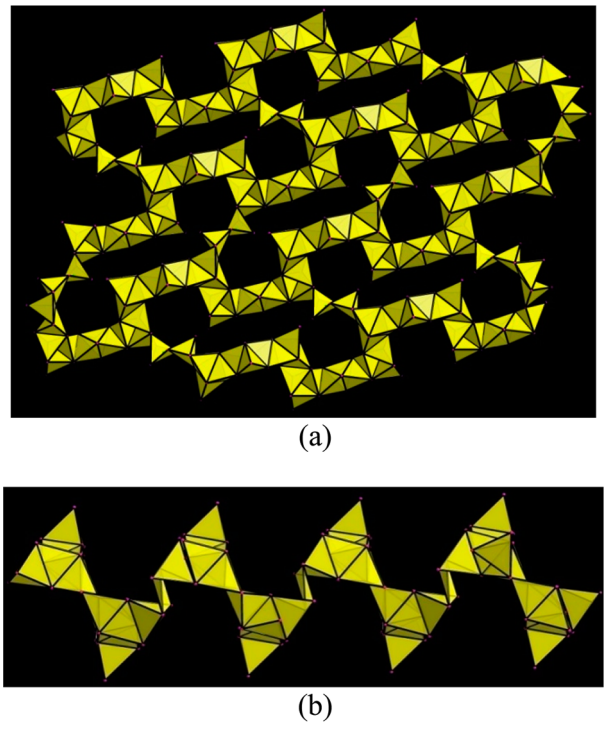

Figure 3. Perspective (a) and side (b) views of 2D herringbone-like networks in **1**.

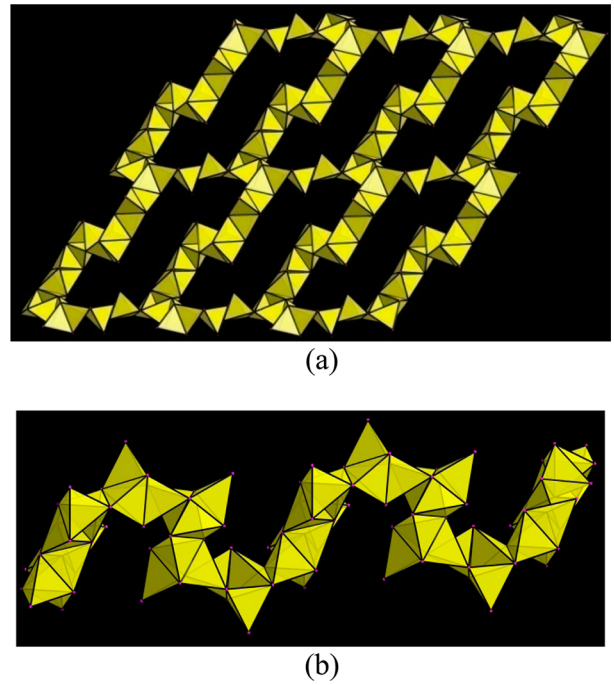

Figure 4. Perspective (a) and side (b) views of a 2D bricklike network in **2**.

compounds could be viewed as reaction-temperature-controlled polymorphs.

Possible Formation Mechanism. The mechanisms of formation of zeolite molecular sieves have been discussed by postulating hierarchical building units in recent years.[7,24] Following the nomenclature in the description of zeolite molecular sieves, a nomenclature scheme to denote the formation of two polymorphs is shown below (Chart 1). It is

dx.doi.org/10.1021/ic500822w | Inorg. Chem. 2014, 53, 8376−8383

Chart 1. Schematic Representation of the Formation of Inorganic Frameworks in Polymorphs 1 and 2

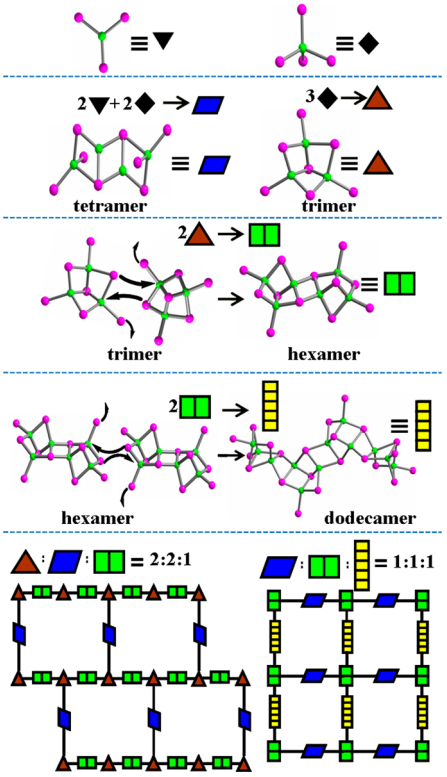

undeniable that CuI_3 triangles and CuI_4 tetrahedra are the initial building units, similar to TO_4 tetrahedra of zeolite molecular sieves, which may self-assemble into layered polymorphs **1** and **2** step by step. Intuitionally, three edge-sharing CuI_4 tetrahedra could result in the Cu_3I_7 trimer, while two CuI_3 triangles and two CuI_4 tetrahedra could fuse into the Cu_4I_8 tetramer. The Cu_3I_7 trimer and Cu_4I_8 tetramer can be viewed as SBUs in the formation of **1** and **2**. Then two Cu_3I_7 SBUs further transform into a Cu_6I_{12} TBU, which can subsequently condense into the $Cu_{12}I_{22}$ QBU. These hierarchical building units with negative charge in the solution might be governed by the alkylated DABCO because of the interactions between positive and negative ions, which lead to infinite condensation and form different topological frameworks. Under the guidance of alkylated cations, Cu_3I_7 SBUs as 3-connected nodes can integrate with hexamers and tetramers to form a (6,3) topological layer with a 24-membered-ring cavity in **1**. Likewise, the Cu_6I_{12} TBUs can be defined as 4-connected nodes, which are linked by dodecamers and tetramers to produce a (4,4)-connected topological layer also with a 24-membered-ring cavity in polymorph **2**. To be noted, the arrangement of hierarchical building units in the formation of **1** and **2** is not arbitrary but a result of minimization of the lattice energy during the condensation, and this kind of self-assemble process is conducted by organic templates.

Photoluminescence and Sensing. As shown in Figure 5a, both **1** and **2** show similar photoluminescence at room temperature in the solid state. It is revealed that a weak high-energy emission and a strong low-energy emission were found in both **1** and **2**. The high-energy emission appears at 448 nm with τ = 90.8 μs for **1** and τ = 21.3 μs for **2** upon excitation at 325 nm, and the strong low-energy green emission band appears at 501 nm (τ = 56.7 μs for **1** and τ = 15.6 μs for **2**).

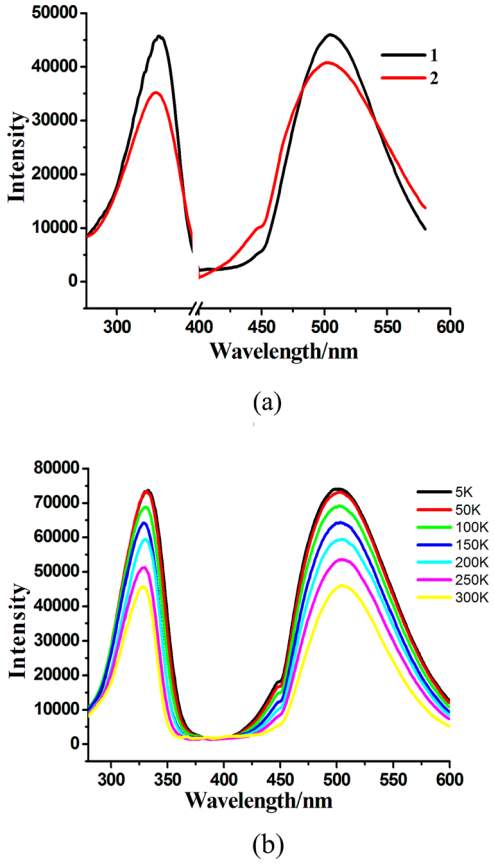

Figure 5. Photoluminescent emissions and excitations of **1** and **2** (a) and solid-state luminescent spectra of **1** under different temperatures (b).

The lifetimes of the emissions determined are similar and relatively long at room temperature, which indicates the strong phosphorescent character. There is a slight discrepancy that the high-energy emission of **1** is more visible than that of **2** at room temperature. Solid-state emission and excitation spectra for two polymorphs have been recorded from room temperature down to 5 K, as can be seen in Figures 5b and S2 in the SI. Along with an decrease of the temperature, no shift is observed on the emission and excitation bands, while the intensity progressively increases. Especially, it is very easily observed that the high-energy emissions become increasingly visible. The photoluminescence property and mechanism of the two polymorphs are similar to those of copper(I) halides, which have been studied by the Ford and Feng groups.[18a,25] The emission bands might be assigned to a triplet "cluster-centered" (^{3}CC) excited state, which has mixed iodide-to-metal charge transfer (^{3}XMCT) and metal-centered transfer (^{3}MC: $d^{10} \rightarrow d^9s^1$Cu) character.

Recently, some metal−organic materials possess luminescence behavior affected by guest molecules that can be used for the sensing of small-molecule pollutants.[26] Thus, to examine the potential of polymorphs toward sensing of small molecules, two polymorphs were selected to investigate the photoluminescent properties in suspension in different organic solvents. The finely grinded samples **1** and **2** (3 mg) were immersed into 3 mL of 1,4-dioxane (Diox), 2-propanol, EtOH, anisole, benzyl alcohol, nitrocarbol, benzaldehyde, and NB, respectively. Each suspension was treated by ultrasonication for 30 min and then aged for 3 days to form a stable emulsion

dx.doi.org/10.1021/ic500822w | Inorg. Chem. 2014, 53, 8376−8383

before the fluorescence measurements. As shown in Figures 6a and S3 in the SI, the emission intensities of two polymorphs

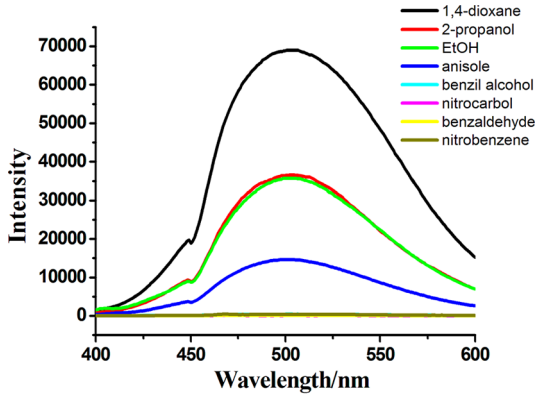

(a)

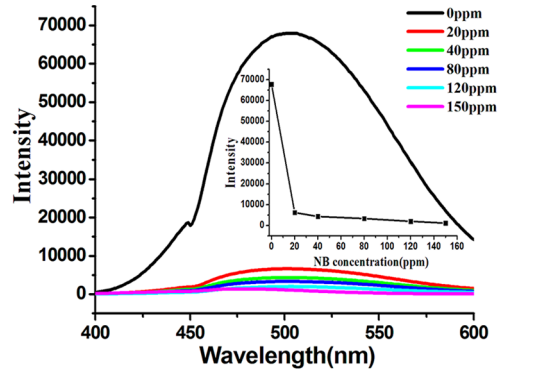

(b)

Figure 6. Emission spectra of **1** (a) in different solvents and (b) at different NB concentrations in Diox (excited at 325 nm). Inset: Corresponding intensity of emission at different NB concentrations.

exhibit solvent-dependent behavior at around 500 nm upon excitation at 325 nm, especially toward the aromatic solvents (except for anisole), which shows a significant quenching effect. Such solvent-dependent quenching behavior might originate from the electron-withdrawing groups of solvents, which can be explained by the donor−acceptor electron-transfer mechanism.[27] Because NB molecules are relevant to explosives, their detection is crucial for security, environmental, and military matters. Thus, the sensing of NB was measured in detail.

To further understand this quenching phenomenon, a batch of **1** in Diox with gradually increasing NB concentration was prepared to monitor the emissive response. The luminescent intensity of the emulsions significantly decreased with increasing NB, and the emission was nearly completely quenched at a concentration of 150 ppm. Detectable luminescence quenching of **1** was observed at a very low concentration of 20 ppm with a very high efficiency of 90.85 and an extremely high detection sensitivity of **1** toward NB. The outstanding sensing capability of **1** may be attributed to its infinite 2D anion framework, which facilitates stronger interaction between NB and the host framework, which affects electron transfer from the excited-state electron-donating anion framework to electron-withdrawing NB.[28] In addition, the sensing of NB by **2** was also examined in detail. The quenching efficiency of **2** with the same NB concentration is slightly lower than that of **1**. Such splendid behaviors make two polymorphs potential candidates for efficiently detecting trace NB.

Photocatalysis. Temperature dependences of the electrical resistivities for pelleted **1** and **2** were measured at 220−300 K; they decrease as the temperature rises and reach about 1.4×10^7 Ω·cm, indicating semiconductor character (Figure S5a in the SI). UV−vis diffuse reflectance of **1** and **2** at room temperature shows band-gap values of 3.2 and 3.1 eV, respectively (Figure S5b in the SI). Band structure calculation of **1** and **2** along with DOS has been carried out with the CASTEP code. The results of the band-gap values are 2.21 and 2.19 eV, respectively, which are a little smaller than the experimental value. The well-known band-gap problem based on Kohn−Sham DFT within the local density of the generalized-gradient approximation contributes to this disagreement.[29] The results indicate that the tops of the valence bands in both compounds are mostly formed by Cu 3d states mixing with I 5p states, while the bottoms of the conduction bands are almost a contribution from I 5s states mixing with Cu 4s states (Figure 7). On the basis of the above calculations, the green photoluminescent emissions of two polymorphs can be assigned as mainly originating from iodine-to-copper charge-transfer (^{3}XMCT) and metal-centered transfer (^{3}MC; d^{10} Cu → d^9s^1 Cu), which is consistent with the previous reports on CuI compounds.[30] Both **1** and **2** have absorption response to

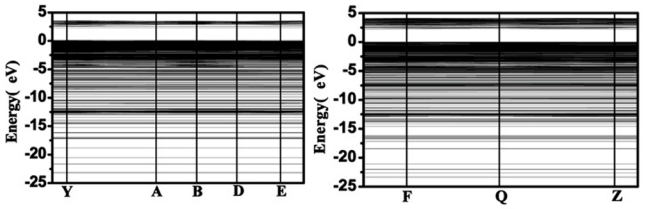

(a)

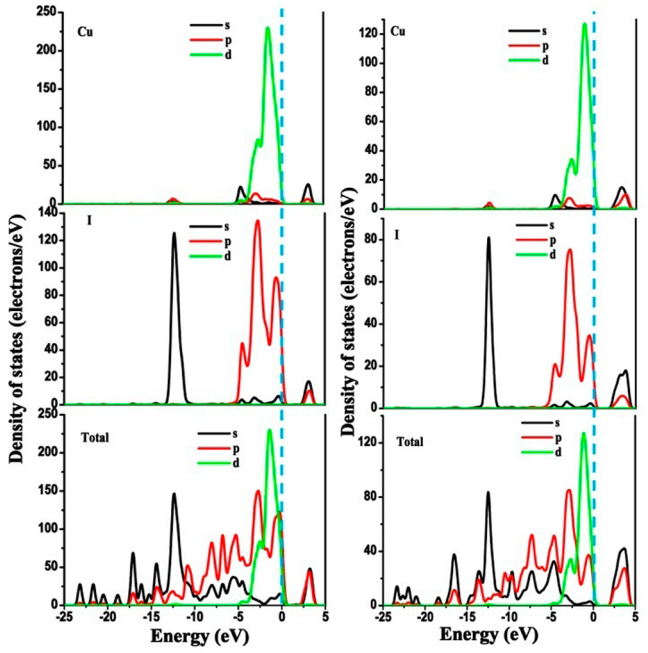

(b)

Figure 7. Energy-band structures (a) and (total and partial) DOS (b) of **1** (left) and **2** (right).

dx.doi.org/10.1021/ic500822w | Inorg. Chem. 2014, 53, 8376−8383

UV light because of their wide-band-gap sizes, which encouraged us to investigate the photocatalytic activities of both isomers. Seven organic dyes were selected for degradation.

The distinct performances on the photocatalytic degradation of organic dyes were discovered in these two polymorphs with such close structural features. Two isomers showed different photocatalytic efficiencies for different organic dyes in an aqueous solution under UV-light irradiation. As shown in Figure S14 in the SI, the residual concentration of dyes in an aqueous solution gradually decreased as a function of the increasing reaction time, indicating that both isomers can degrade all of the seven organic dyes. First, for the degradation of MB, the photocatalytic degradation process was monitored by UV−vis absorption spectroscopy, which presented distinct adsorption. A comparison of the photocatalytic activities of two isomers exhibits that the degradation of MB is highly efficient and the ratio of the degradation reaches about 97%. To prove the high photocatalytic efficiency of **1** and **2** to MB, comparative experiments without catalyst under UV-light irradiation were performed, which only showed very little decomposition. We had also studied the photocatalytic activity of CuI to MB under similar conditions, which showed that the rate of degradation was still very slow (Figure S14 in the SI). To further check the photocatalytic activities of two polymorphs, similar procedures were performed upon degradation of NR, ED, AI, MO, MG, and EY (Figures 8 and S6−S13 in the SI). For photocatalyst **1**, the degradation ability is nearly the same as that of **2** except that the degradation ratio and speed of ED are very different. It is obvious that **1** exhibits much lower photocatalytic activity of ED. The degradation ratio of ED only reaches 32% in 150 min, while for compound **2**, the corresponding ratio can reach 85%. The degraded speed of other dyes for two isomers is different, but the degraded rate is almost similar after prolonged irradiation. The reason why the discrepancy in the photocatalytic activity occurs between **1** and **2** should be related to the slight structural difference, but it is difficult to explain at the current stage.

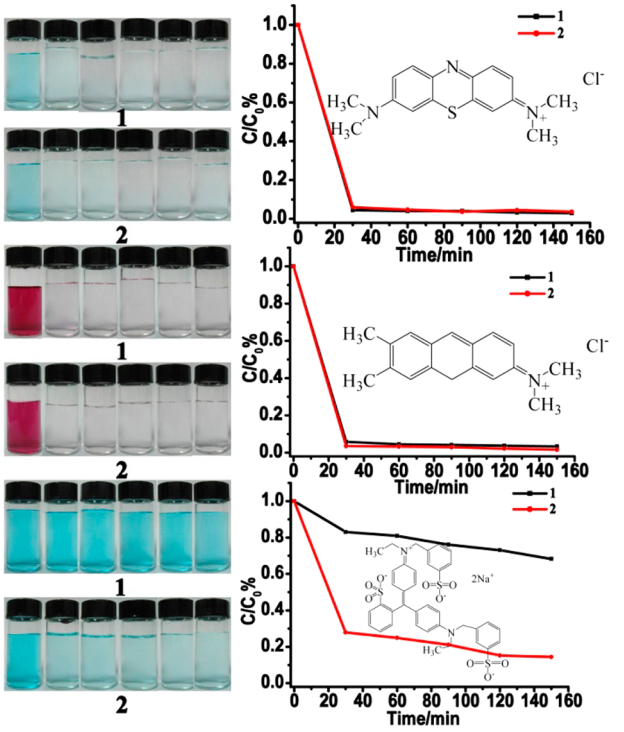

Figure 8. Photodecomposition of three dyes (a, MB; b, NR; c, ED) in solution over two polymorphs. Left: Color change photograph image of a dye solution. Right: Ratio of the remaining three dyes with time in the presence of two isomeric photocatalysts monitored by UV−vis spectra.

To further demonstrate the efficiency and versatility of catalyst **1**, a light-blue solution of ED and a light-red solution of NR were mixed thoroughly to form a purple solution, to which **1** was added and then exposed to UV irradiation. The degradation process was monitored by UV−vis absorption spectroscopy, which varied with the photocatalytic time. When the light application time increased to 30 min, the color of the solution turned light blue from purple and essentially came to the color of the residual ED, which was reflected by UV−vis spectroscopy (Figure 9). It is further proven that the degradation efficiency of NR for **1** was much higher than that of ED. Both photocatalysts **1** and **2** show a high UV-light-driven photocatalytic efficiency, which is the first application in photocatalytic degradation of dyes for copper(I) iodide polymorphs. In order to investigate the integrity of two polymophs as UV-light photocatalysts, the catalysts were recovered from reaction solutions via simple filtration. For the degradation of MB, the results show that about 27 mg (90%) of catalysts can be recovered. The small amount of loss may be due to the unavoidable solubility of the sample and relatively simple filtration process. The PXRD patterns of the recovered samples after photodegradation are still in agreement with that of the as-prepared sample (Figure S15 in the SI), indicating that two isomers maintain their structural integrity.

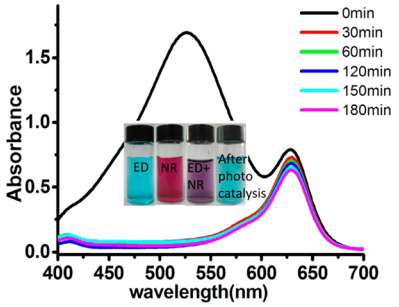

Figure 9. Time-dependent UV−vis spectra of a NR and ED mixture in the presence of **1**. Inset: Corresponding photographs of photodegradation.

CONCLUSION

In summary, two semiconducting isomeric copper(I) iodide hybrid materials with alkylated DABCO cations were successfully synthesized under different temperatures. To the best of our knowledge, these two polymorphs are the first examples of 2D inorganic iodocuprate framework polymorphs that exhibit similar basic building units and 24-membered-ring cavities but different CuI structural motifs (herringbone-like and bricklike networks). It should be possible to probe copper(I) halide aggregates and their structures in greater detail to elucidate the self-assembly process. On the basis of this consideration, we have proposed a new model for forming and assembling copper halide frameworks by observation of hierarchical units in these two polymorphs. Photoluminescent spectra in different solvents demonstrate that two polymorphs exhibit distinct solvent-dependent photoluminescence emis-

dx.doi.org/10.1021/ic500822w | Inorg. Chem. 2014, 53, 8376−8383

sions and highly sensitive sensing of NB explosives. Two polymorphs exhibit extremely highly efficient photocatalytic decomposition of organic pollutants, which is the first example of cuprous iodide polymorphs with photocatalytic application. These results provide an opening into a promising new field of the highly efficient photocatalytic degradation pollutant.

■ ASSOCIATED CONTENT

Supporting Information

Additional figures, UV−vis diffuse-reflectance spectrum, and PXRD, detailed photodecomposition analyses, and crystallographic CIF data for **1** and **2**. This material is available free of charge via the Internet at http://pubs.acs.org.

■ AUTHOR INFORMATION

Corresponding Author

*E-mail: zhangxm@dns.sxnu.edu.cn. Fax: +86 357 2051402.

Notes

The authors declare no competing financial interest.

■ ACKNOWLEDGMENTS

This work was financially supported by the 973 Program (Grant 2012CB821701), the Ministry of Education of China (Grant IRT1156), the National Science Fund for Distinguished Young Scholars (Grant 20925101), and the Graduate Education Innovation Project of Shanxi Province (20103061).

■ REFERENCES

(1) (a) Moulton, B.; Zaworotko, M. J. *Chem. Rev.* **2001**, *101*, 1629−1658. (b) Skořepová, E.; Čejka, J.; Hušák, M.; Eigner, V.; Rohlíček, J.; Šturc, A.; Kratochvíl, B. *Cryst. Growth Des.* **2013**, *13*, 5193−5203. (c) Wen, T.; Zhang, D.-X.; Zhang, J. *Inorg. Chem.* **2013**, *52*, 12−14.

(2) Ting, V. P.; Schmidtmann, M.; Wilson, C. C.; Weller, M. T. *Angew. Chem., Int. Ed.* **2010**, *49*, 9408−9411.

(3) (a) Cantín, Á.; Corma, A.; Díaz-Cabañas, M. J.; Jordá, J. L.; Moliner, M.; Rey, F. *Angew. Chem.* **2006**, *118*, 8181−8183. (b) Davis, M. E. *Nature* **2002**, *417*, 813−821.

(4) (a) Li, J.; Papadopoulos, C.; Xu, J. *Nature* **1999**, *402*, 253−254. (b) lijima, S. *Nature* **1991**, *354*, 56−58.

(5) Martinez-Lillo, J.; Armentano, D.; Mastropietro, T. F.; Julve, M.; Faus, J.; De Munno, G. *Cryst. Growth Des.* **2011**, *11*, 1733−1741.

(6) (a) Umemura, A.; Diring, S.; Furukawa, S.; Uehara, H.; Tsuruoka, T.; Kitagawa, S. *J. Am. Chem. Soc.* **2011**, *133*, 15506−15513. (b) Morris, R. E. *ChemPhysChem* **2009**, *10*, 327−329.

(7) (a) Murugavel, R.; Walawalkar, M. G.; Dan, M.; Roesky, H. W.; Rao, C. N. R. *Acc. Chem. Res.* **2004**, *37*, 763−774. (b) Oliver, S.; Kuperman, A.; Ozin, G. A. *Angew. Chem., Int. Ed.* **1998**, *37*, 46−62.

(8) Corma, A.; Navarro, M. T.; Rey, F.; Rius, J.; Valencia, S. *Angew. Chem.* **2001**, *113*, 2337−2340.

(9) (a) Rojas, A.; Arteaga, O.; Kahr, B.; Camblor, M. A. *J. Am. Chem. Soc.* **2013**, *135*, 11975−11984. (b) Lobo, R. F.; Tsapatsis, M.; Freyhardt, C. C.; Chan, I.; Chen, C.-Y.; Zones, S. I.; Davis, M. E. *J. Am. Chem. Soc.* **1997**, *119*, 3732−3744. (c) Rojas, A.; Camblor, M. A. *Angew. Chem.* **2012**, *124*, 3920−3922.

(10) (a) Neuba, A.; Haase, R.; Meyer-Klaucke, W.; Flörke, U.; Henkel, G. *Angew. Chem., Int. Ed.* **2012**, *51*, 1714−718. (b) Haldón, E.; Álvarez, E.; Nicasio, M. C.; Pérez, P. J. *Inorg. Chem.* **2012**, *51*, 8298−8306. (c) Monnier, F.; Taillefer, M. *Angew. Chem., Int. Ed.* **2009**, *48*, 6954−6971. (d) Díez-González, S.; Marion, N.; Nolan, S. P. *Chem. Rev.* **2009**, *109*, 3612−3676. (e) Perruchas, S.; Goff, X. F. L.; Maron, S.; Maurin, I.; Guillen, F.; Garcia, A.; Gacoin, T.; Boilot, J.-P. *J. Am. Chem. Soc.* **2010**, *132*, 10967−10969. (f) Eperon, G. E.; Stranks, S. D.; Menelaou, C.; Johnston, M. B.; Herz, L. M.; Snaith, H. J. *Energy Environ. Sci.* **2014**, *7*, 982−988. (g) Li, M.; Li, Z.; Li, D. *Chem. Commun.* **2008**, 3390−3392.

(11) (a) Lu, J. Y.; Cabrera, B. R.; Wang, R.-J.; Li, J. *Inorg. Chem.* **1999**, *38*, 4608−4611. (b) Graham, P. M.; Pike, R. D. *Inorg. Chem.* **2000**, *39*, 5121−5132. (c) Liu, Z.-W; Qayyum, M. F.; Wu, C.; Whited, M. T.; Djurovich, P. I.; Hodgson, K. O.; Hedman, B.; Solomon, E. I.; Thompson, M. E. *J. Am. Chem. Soc.* **2011**, *133*, 3700−3703.

(12) Hu, M.-C.; Wang, Y.; Zhai, Q.-G.; Li, S.-N.; Jiang, Y.-C.; Zhang, Y. *Inorg. Chem.* **2009**, *48*, 1449−1468.

(13) Mishra, S.; Jeanneau, E.; Ledoux, G.; Daniele, S. *CrystEngComm* **2012**, *14*, 3894−3901.

(14) Hou, J.-J.; Li, S.-L; Li, C.-R.; Zhang, X.-M. *Dalton Trans.* **2010**, *39*, 2701−2707.

(15) (a) Lee, J. Y.; Kim, H. J.; Jung, J. H.; Sim, W.; Lee, S. S. *J. Am. Chem. Soc.* **2008**, *130*, 13838−13839. (b) Harvey, P. D.; Knorr, M. *Macromol. Rapid Commun.* **2010**, *31*, 808−826.

(16) DeBord, J. R. D.; Lu, Y.-j.; Warren, C. J.; Haushalter, R. C.; Zubieta, J. *Chem. Commun.* **1997**, 1365−1366.

(17) Li, Q.-Y; Fu, Y.-L *CrystEngComm* **2009**, *11*, 1515−1518.

(18) (a) Bi, M.-H.; Li, G.-H.; Hua, J.; Liu, Y.-L.; Liu, X.-M.; Hu, Y.-W.; Shi, Z.; Feng, S.-H. *Cryst. Growth Des.* **2007**, *7*, 2066−2070. (b) Wu, T.; Li, M.; Li, D.; Huang, X.-C. *Cryst. Growth Des.* **2007**, *8*, 568−574.

(19) (a) Segall, M.; Linda, P.; Probert, M.; Pickard, C.; Hasnip, P.; Clark, S.; Payne, M. *Materials Studio CASTEP*, version 2.2; Accelrys: San Diego, CA, 2002. (b) Segall, M.; Linda, P.; Probert, M.; Pickard, C.; Hasnip, P.; Clark, S.; Payne, M. *J. Phys.: Condens. Matter* **2002**, *14*, 2717−2744.

(20) (a) Peng, R.; Li, M.; Li, D. *Coord. Chem. Rev.* **2010**, *254*, 1−18. (b) Chen, J.-K.; Yao, Y.-G.; Zhang, J.; Li, Z.-J; Cai, Z.-W.; Zhang, X.-Y.; Chen, Z.-N.; Chen, Y.-B.; Yao, K.; Qin, Y.-Y.; Wen, Y.-H. *J. Am. Chem. Soc.* **2004**, *126*, 7796−7797. (c) Xin, B.-J.; Li, Y.; Zeng, G.; Peng, Y.; Li, G.-H.; Shi, Z.; Feng, S.-H. *Z. Anorg. Allg. Chem.* **2013**, *639*, 611−617.

(21) (a) Haddad, S.; Willett, R. D. *Inorg. Chem.* **2001**, *40*, 2457−2460. (b) Li, S.-L.; Zhang, R.; Hou, J.-J.; Zhang, X.-M. *Inorg. Chem. Commun.* **2013**, *32*, 12−17.

(22) Mishra, S.; Jeanneau, E.; Chermette, H.; Daniele, S.; Hubert-Pfalzgraf, L. G. *Dalton Trans.* **2008**, 620−630.

(23) (a) Lommerse, J. P. M.; Stone, A. J.; Taylor, R.; Allen, H. *J. Am. Chem. Soc.* **1996**, *118*, 3108−3116. (b) Yin, Z.; Wang, Q.-X.; Zeng, M.-H. *J. Am. Chem. Soc.* **2012**, *134*, 4857−4863.

(24) (a) Rao, C. N. R.; Natarajan, S.; Choudhury, A.; Neeraj, S.; Ayi, A. A. *Acc. Chem. Res.* **2001**, *34*, 80−87. (b) Férey, G. *J. Fluorine Chem.* **1995**, *72*, 187−193.

(25) (a) Ford, P. C.; Cariati, E.; Bourassa, J. *Chem. Rev.* **1999**, *99*, 3625−3648. (b) Bi, M.-H.; Li, G.-H.; Zou, Y.-C.; Shi, Z.; Feng, S.-H. *Inorg. Chem.* **2007**, *46*, 604−606.

(26) (a) Cui, Y.-J.; Yue, Y.-F.; Qian, G.-D.; Chen, B.-L. *Chem. Rev.* **2011**, *112*, 1126−1162. (b) Wang, H.; Yang, W.-T.; Sun, Z.-M. *Chem.—Asian J.* **2013**, *8*, 982−989.

(27) Pramanik, S.; Zheng, C.; Zhang, X.; Emge, T. J.; Li, J. *J. Am. Chem. Soc.* **2011**, *133*, 4153−4155.

(28) (a) Chen, B.-L.; Wang, L.-B.; Xiao, Y.-Q.; Fronczek, F. R.; Xue, M.; Cui, Y.-J.; Qian, G.-D. *Angew. Chem., Int. Ed.* **2009**, *48*, 500−503. (b) Lan, A.-J.; Li, K.-H.; Wu, H.-H.; Olson, D. H.; Emge, T. J.; Ki, W.; Hong, M.-H.; Li, J. *Angew. Chem., Int. Ed.* **2009**, *48*, 2334−2338.

(29) (a) Perdew, J. P.; Levy, M. *Phys. Rev. Lett.* **1983**, *51*, 1884−1887. (b) Yang, J.; Dolg, M. *J. Phys. Chem. B* **2006**, *110*, 19254−19263.

(30) (a) Kyle, K. R.; Ryu, C. K.; DiBenedetto, J. A.; Ford, P. C. *J. Am. Chem. Soc.* **1991**, *113*, 2954−2965. (b) Cariati, E.; Bu, X.; Ford, P. C. *Chem. Mater.* **2000**, *12*, 3385−3391. (c) Zhang, Y.; Wu, T.; Liu, R.; Dou, T.; Bu, X.-H.; Feng, P.-Y. *Cryst. Growth Des.* **2010**, *10*, 2047−2049. (d) Wu, T.; Li, D.; Ng, S. W. *CrystEngComm* **2005**, *7*, 514−518.